Figure S1. Iron import in pathogenic *Neisseria*. a. Iron uptake from hTf presumably begins by formation of a TbpB-(holo)hTf (blue/yellow) complex on the bacterial cell surface. The complex then binds to TbpA, a TonB-dependent iron transporter (green). Transport of ferric iron across the OM is driven by energy from the inner membrane proton motive force. This requires physical contact with an energy-transducing TonB complex in the inner membrane (IM), consisting of TonB, ExbB and ExbD proteins (labeled TONB, pink). Upon transport across the OM, ferric iron is bound by FbpA, a periplasmic binding protein (gray), and then transported across the IM by an ABC transporter (gold).
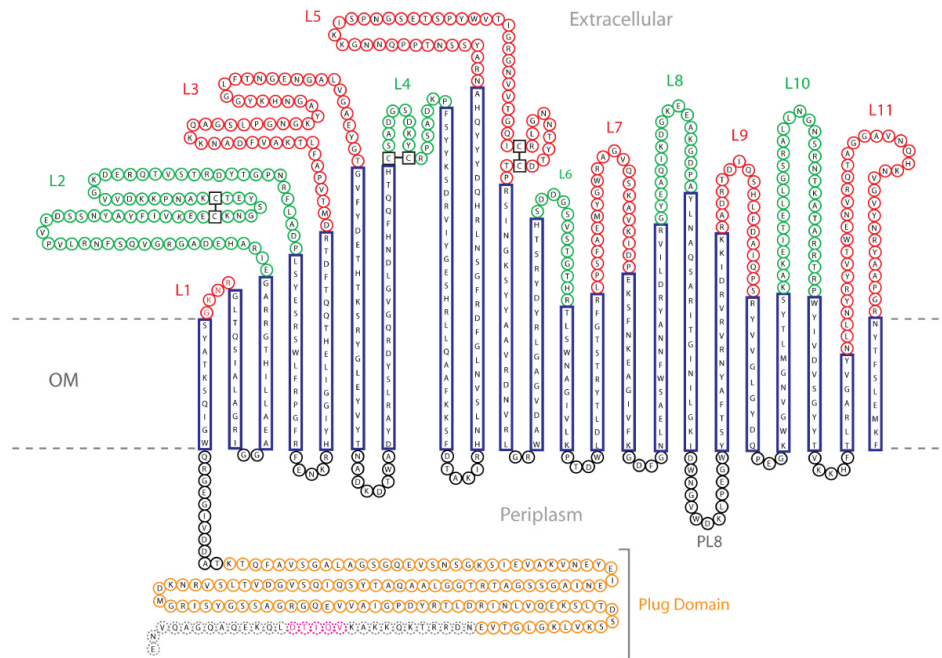
Figure S2. Topology diagram of TbpA from *N. meningitidis* strain K454 (serogroup B). **a**. Topology of TbpA with β strands are shown in blue, periplasmic loops in black, plug domain in gold (no secondary structure is depicted), disordered residues (including the TonB box, shown in magenta) in gray, and extracellular loops alternating in green and red (for clarity). TbpA is the largest TonB-dependent transporter with known structure, with most of the additional mass found in extracellular loops 2 (76 residues), 3 (54 residues), 5 (54 residues), 10 (31 residues), and 11 (38 residues). While most β-strand connections on the periplasmic side of the OM are short, there is one periplasmic loop connecting strands 16 and 17 that contains 13 residues and is disordered in the structure.
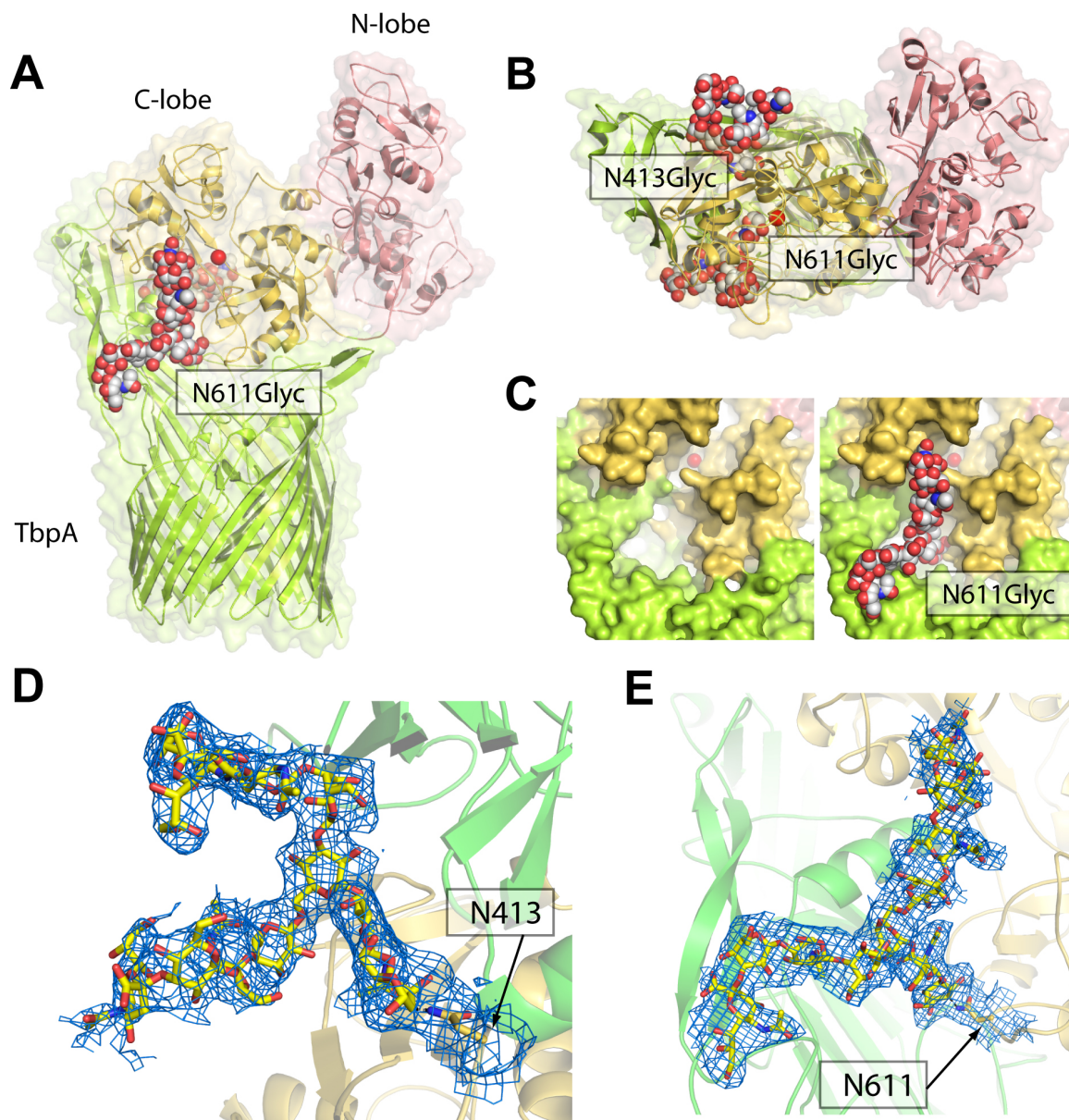
Figure S3: The N-linked glycosylation sites of hTf within the TbpA-hTf crystal structure. **A** and **B**. Two N-linked glycosylation sites were observed in our TbpA-hTf full length crystal structure corresponding to known sites at N413 (electron density shown in panel **D**) and N611 (electron density shown in panel **E**). **C**. *Left*, the N611 glycosylation has been removed to show the cleft formed upon hTf binding. The relative placement of the iron is shown as a red sphere for reference. *Right*, the N611 glycosylation is shown as spheres as it is observed in our crystal structure forming a pseudo wall (analogous to the proposed role of TbpB) which may serve important roles in both preventing iron diffusion and directing iron through the barrel domain of TbpA. Electron density maps are 2Fo-Fc maps contoured at 0.75σ.

conserved K/R

Variable ▬▬▬▬▬▬▬▬▬▬▬▬▬▬ Conserved
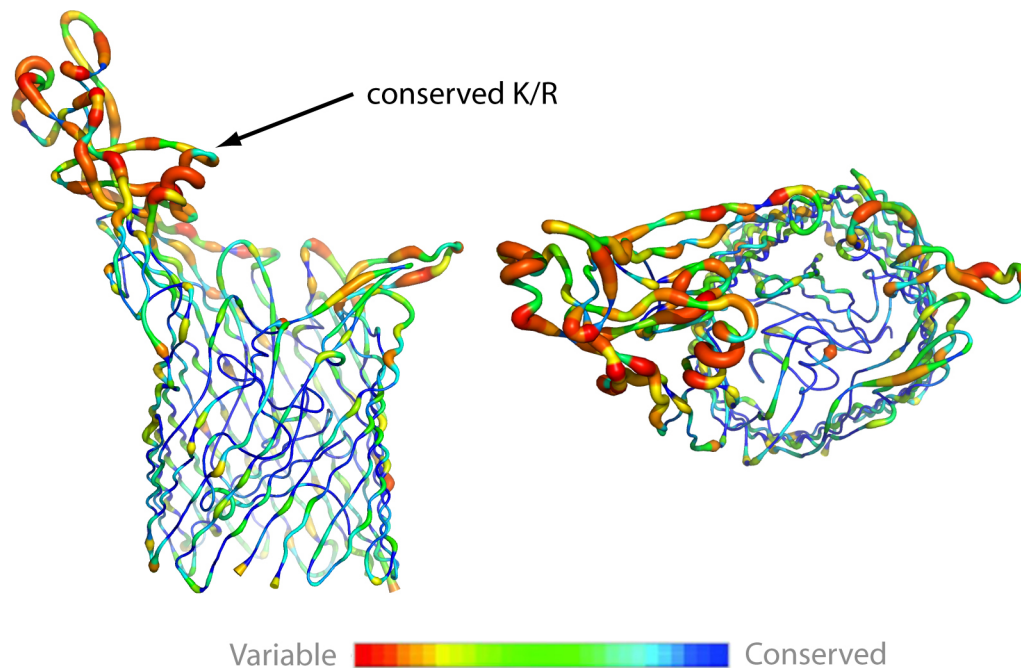
Figure S4: Sequence variability of TbpA extracellular loops. Based on the sequence alignment in Figure S2, conservation scores were calculated and mapped onto the structure of TbpA using the Consurf[1] server and visualized using PyMOL (Schrödinger, LLC). A conservation putty representation shows the loop regions of TbpA to be the most variable (thick red) with the conserved TonB-dependent transporter core (22-stranded beta-barrel and plug domain) being the least variable (thin blue). The helix finger of loop 3 is one of the most variable regions of TbpA and our crystal structures have suggested it may be involved in species selectivity and catalyzing iron release via a K/R residue located at the tip. Note that while the loop 3 helix finger is mostly variable, the K/R residue is well conserved.
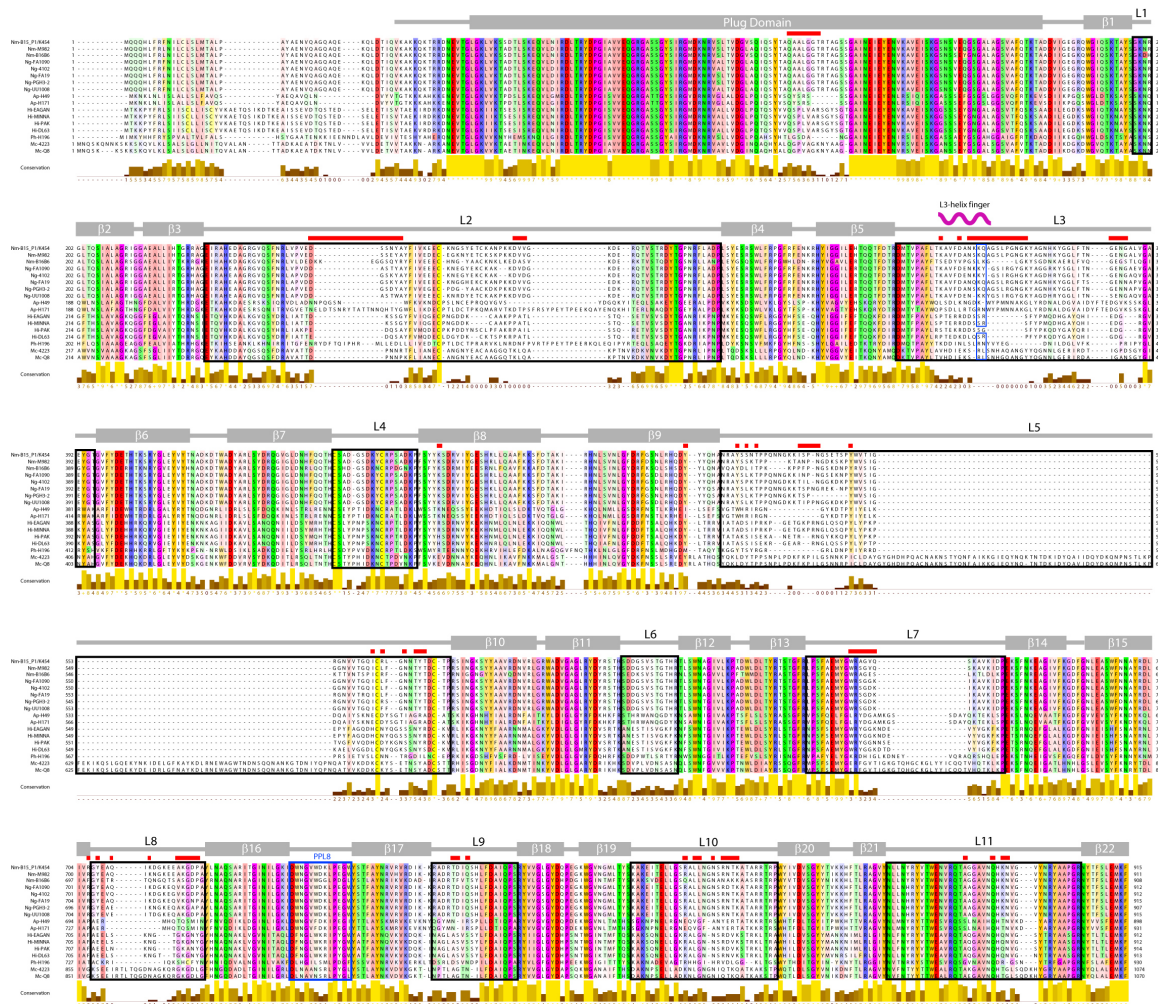
Figure S5: **Sequence alignment of TbpA sequences from known pathogens.** Domain structure is show above the sequence alignment in gray and conservation scores (Jalview[2]) are shown below. The residues are color coded based on both their properties and conservation. Beta-stands (β), loops (L), and the plug domain are labeled accordingly. Loops represent the most variable regions of the alignment and have been outlined in black boxes. Residues which were found to interact with hTf in our TbpA-hTf crystal structure are indicated by red squares above the sequence. The helix finger in loop 3 (L3 helix finger) is shown as a magenta wave. Within this region, we have also outlined in blue the location of the conserved K/R residue that we propose to be responsible for catalyzing iron release. The disordered periplasmic loop 8 (PPL8) is outlined by a blue box and may represent a docking site for FbpA. This loop was disordered in both of our complex structures and is longer than in other TonB-dependent transporters. Abbreviations: *Neisseria meningitidis* (Nm); *Neisseria gonorrhoeae* (Ng); *Haemophilus influenzae* (Hi); *Actinobacillus pleuropneumoniae* (Ap); *Pasteurella haemolytica* (Ph); *Moraxella catarrhalis* (Mc). Adapted from Cornelissen et al[3].
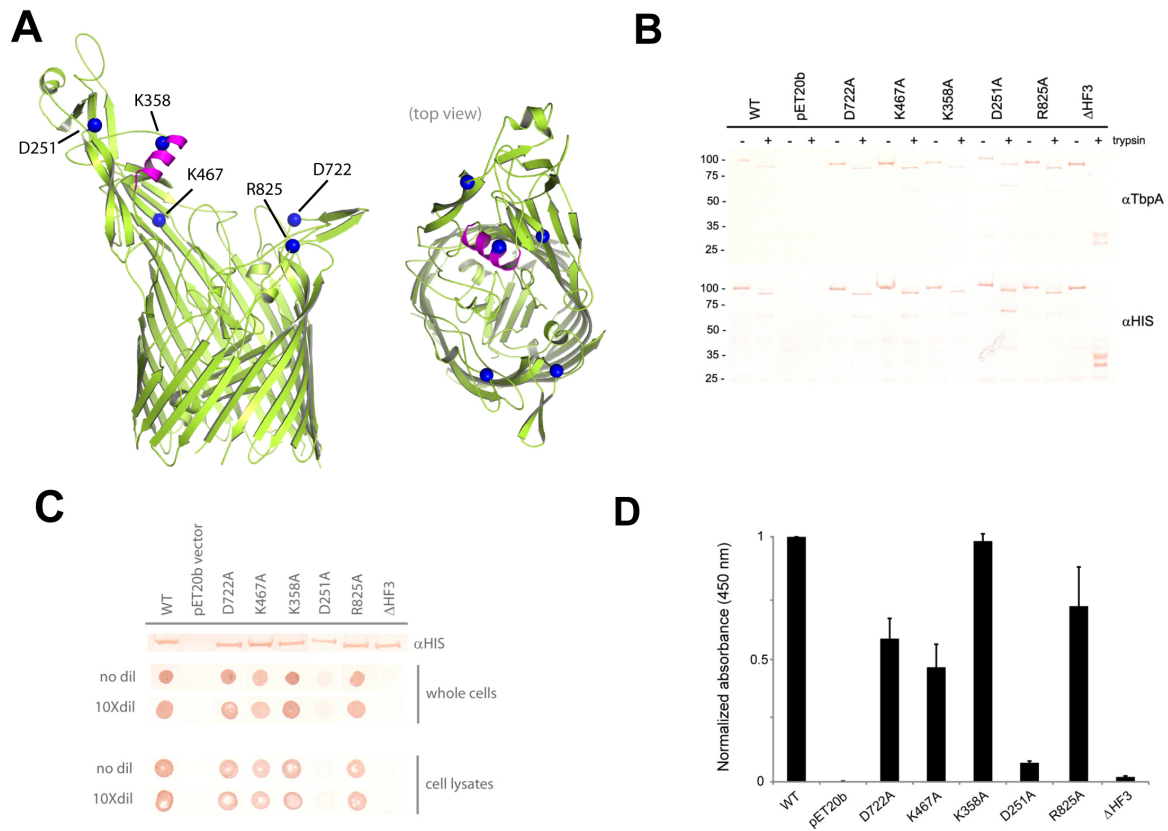
Figure S6: The TbpA and hTf interaction is relatively insensitive to single point mutations. A. Shown is the TbpA structure in green ribbon and the loop 3 helix finger in magenta. The locations of mutations designed to disrupt hTf binding are shown as blue spheres. **B**. A surface shaving assay was performed using trypsin to assess proper folding and surface exposure. Western blots (using both monoclonal anti-His and polyclonal anti-TbpA antibodies) were performed to detect a band shift that indicates proper routing to the surface of the outer membrane. As shown in the blot, a band shift was observed for all of the mutants verifying surface exposure. Interestingly, removing the helix finger of loop 3 appears to lead to the exposure of other protease sites, resulting in a different cleavage profile. **C**. A dot blot assay was performed to probe whether these TbpA mutants could still bind hTf in whole cells (top) and in cell lysates (bottom). The results show that most of the mutations did not significantly affect hTf binding. However, a near elimination of binding was observed in the D251A mutant, which is located in loop 2. Interestingly, removing the helix finger in loop 3 leads to a complete loss of hTf binding, providing further evidence for a crucial role of this striking feature of TbpA. **D**. An ELISA assay using whole cells was performed to probe hTf binding. Results from the ELISA assay and from the dot blot assay (**C**) agree well with one another, again showing the loop 2 mutant D251A greatly reducing hTf binding and elimination of binding with removal of the helix finger in loop 3.
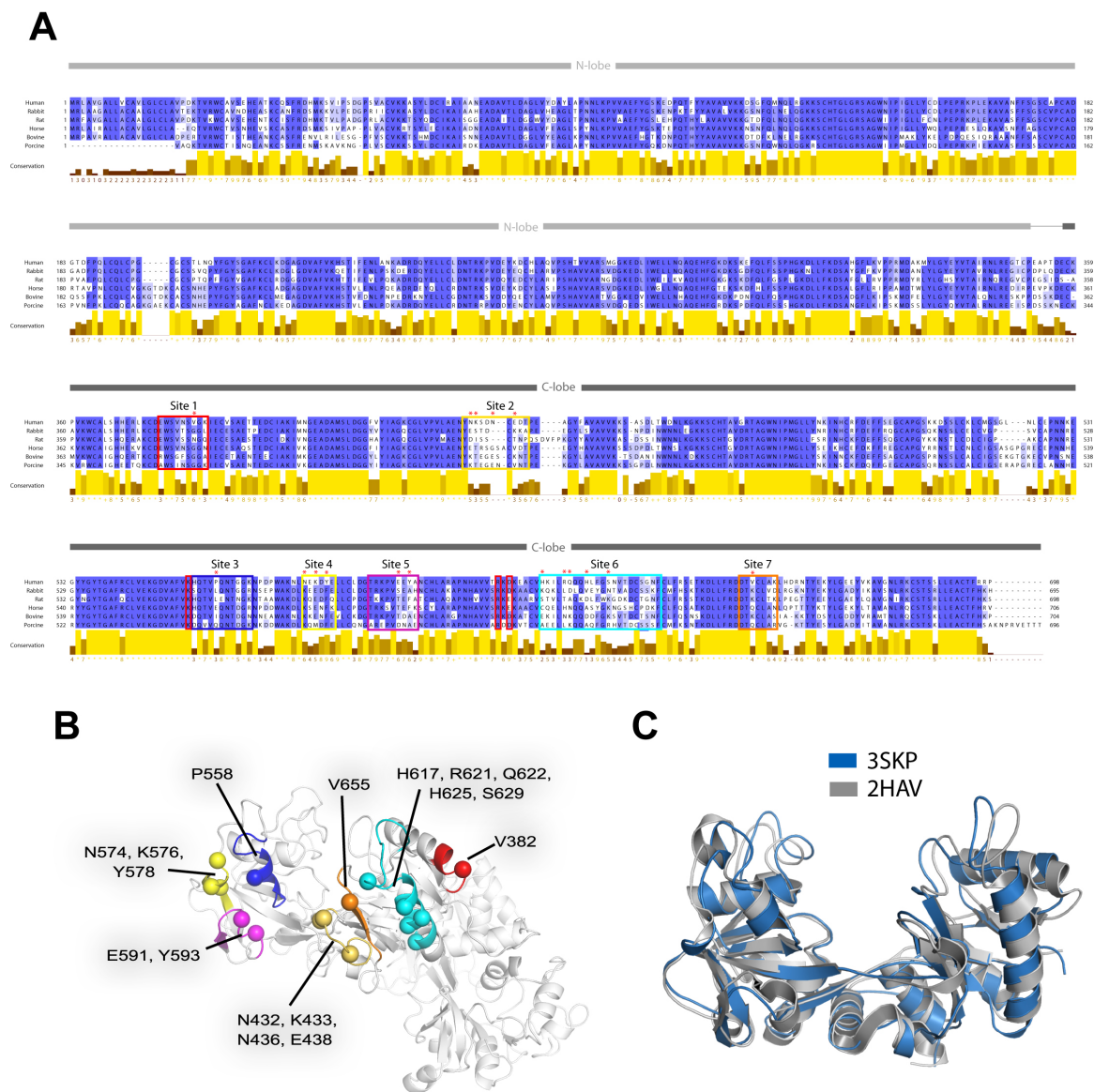
Figure S7: Sequence analysis of transferrins based on the TbpA-(apo)hTf crystal structures. A. Sequence alignment of transferrins from human, rabbit, rat, horse, bovine and porcine. The residues are colored according to conservation and conservation scores (Jalview) are shown below. The N-lobe (gray) and C-lobe (charcoal) domains are indicated above the sequences. Based on our TbpA-hTf crystal structures, we mapped those residues found to interact with TbpA to seven different sites on the C-lobe sequence and these are outlined in black boxes and color coded in panel **B**. Interestingly, these sites also overlap with variable regions found within the C-lobe. Those residues found to interact with TbpA and unique to human Tf are indicated by red asterisks and show as spheres in panel **B**. The conserved C-lobe triad of residues, responsible for sensing the environmental pH (K534, R632, D634), are outlined in red boxes. **C**. Structural alignment of our new C-lobe structure at 1.7 Å (PDB code 3SKP) with the C-lobe from the previously reported full-length (apo)hTf structure at 2.7 Å (PDB code 2HAV).
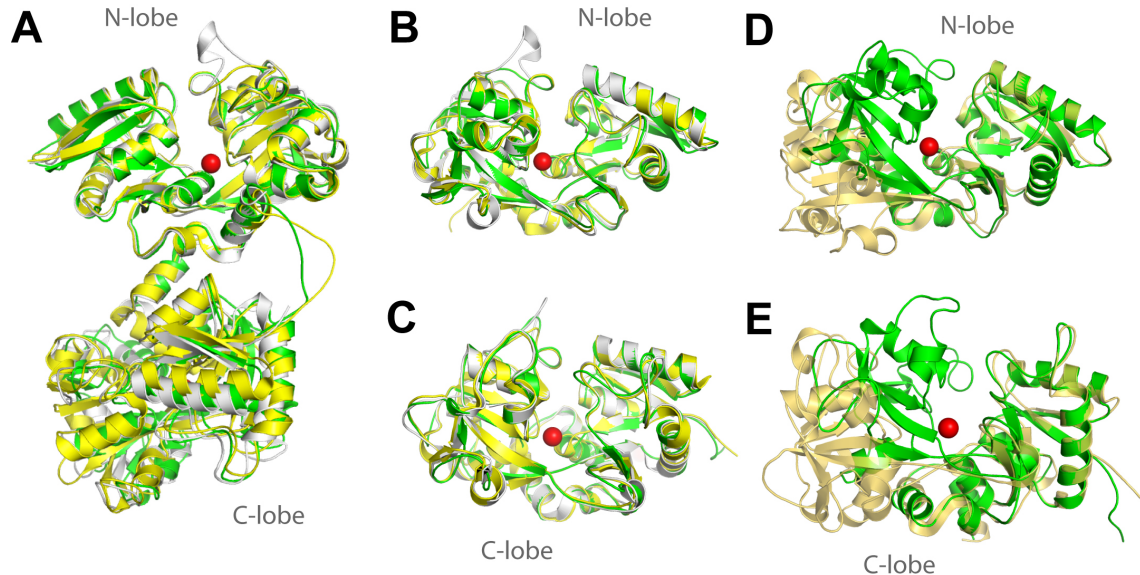
Figure S8: Crystal structure of diferric human transferrin. A. Crystal structure of diferric human transferrin (PDB code 3V83, green) aligned to porcine transferrin (PDB code 1H76, gray, 71% identical) and rabbit transferrin (PDB code 1JNF, yellow, 81% identical) (aligned along the N-lobe). **B**. Comparison of N-lobe conformations of diferric human Tf to porcine (RMSD of 0.465 Å) and rabbit (RMSD of 0.466 Å) diferric Tf. **C**. Comparison of C-lobe conformations of diferric human Tf to porcine (RMSD of 0.421 Å) and rabbit (RMSD of 0.413 Å) transferrins. **D**. Conformational changes within the N-lobes of the apo (gold) and holo (green) human Tf structures (aligned along the N1 domain). **E**. Conformational changes within the C-lobes of the apo (gold) and holo (green) human Tf structures (aligned along the C1 domain).
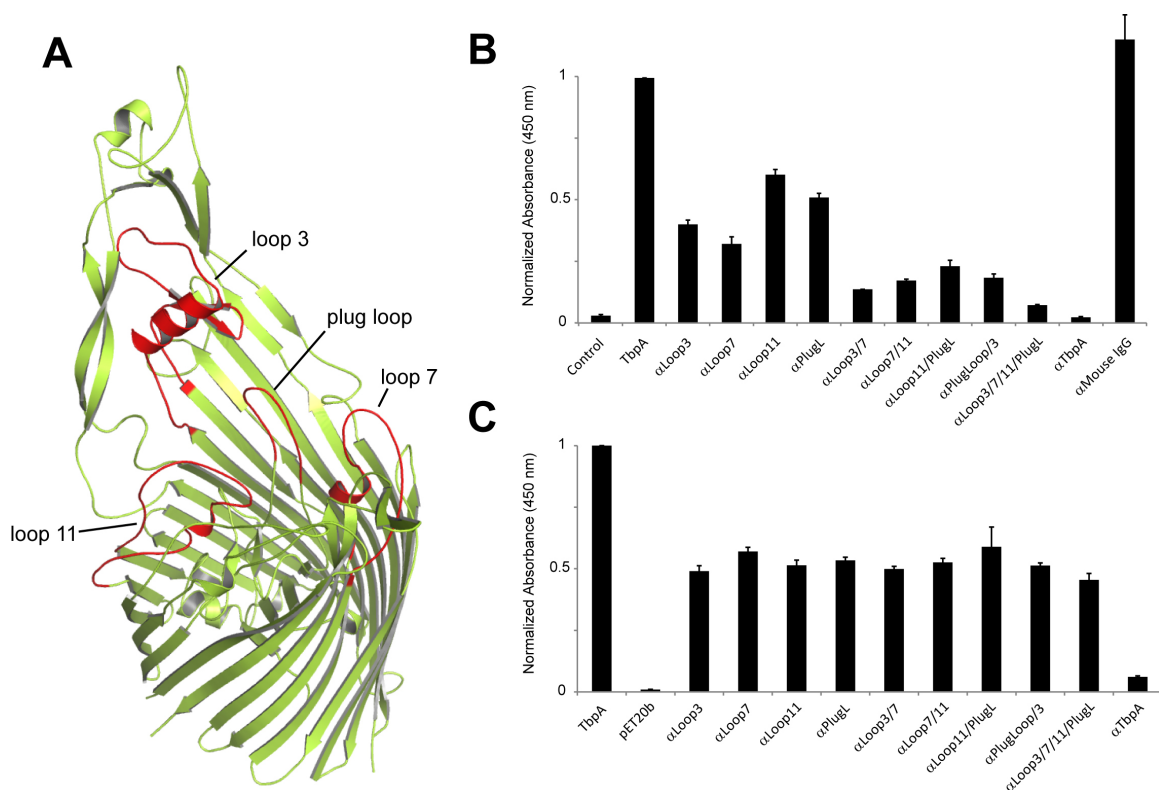
Figure S9: Polyclonal antibodies against TbpA block hTf binding. A. Based on analysis of our crystal structures, we designed peptides representing the plug loop, loop 3, loop 7 and loop 11. These peptides (and full length TbpA) were then used as antigens for polyclonal antibody development in mice. **B**. ELISA assays were used to determine if the antibodies could block hTf binding using purified TbpA. The results show ~50% reduction in binding was observed for each antibody alone and that used in pairs, a >75% reduction in binding was observed, while the anti-TbpA polyclonal antibody completely blocked hTf binding. **C**. A similar ELISA assay as in panel **B** was then performed using whole cells. The results show ~50% reduction in hTf binding for the antibodies targeting the loops, but again, almost complete elimination of binding for the anti-TbpA antibodies.

Full length hTf C-lobe only
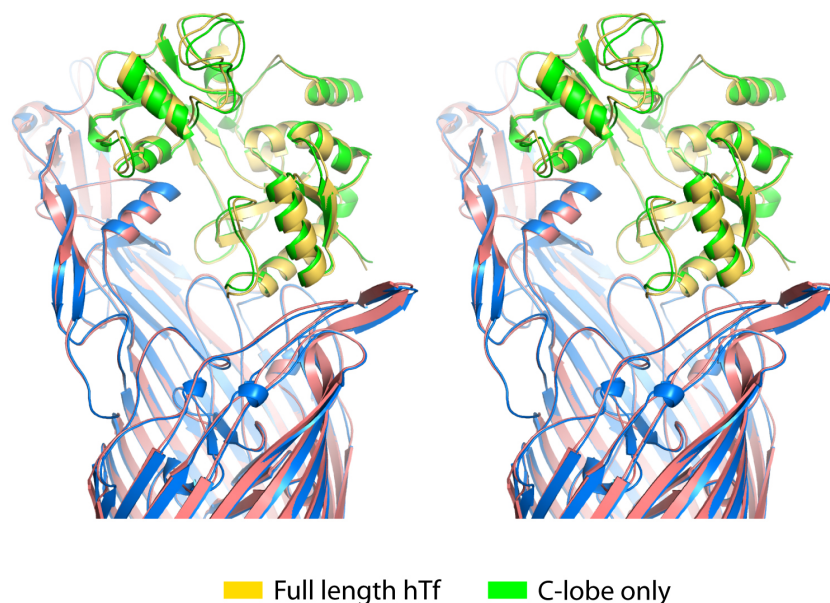
Figure S10: Comparison of the TbpA-(Apo)hTf and TbpA-(apo)hTf C-lobe crystal structures. To confirm that the partially open C-lobe conformation is not an artifact of crystal packing, we determined a 3.2Å structure of TbpA in complex with apo hTf C-lobe (see also Supplementary Fig. 15, Supplementary Table 1). In this new structure, the cleft between the C1- and C2-subdomains is again partially open, with the TbpA helix finger inserted between them. As a further control, we determined a 1.7Å structure of apo hTf C-lobe under different conditions from the original full-length apo hTf structure, and found the C1- and C2-subdomains separated by nearly 50° as the full-length apo structure (Supplementary Fig. 6c, 16, Supplementary Table 1). These experiments indicate that the C-lobe conformations we observe for apo hTf (open) and hTf bound to TbpA (partially open) are physiologically relevant and result from the binding of hTf to TbpA. Figure S8 shows a stereo view of the alignment of the two TbpA-hTf crystal structures (C-lobe from the full length structure is shown in gold (TbpA in blue) and C-lobe only is shown in green (TbpA in light red)). Despite using different constructs and having different packing, the structures overlap almost perfectly with an RMSD of 0.90 Å. The only global difference between the two structures is a slight closing of the C-lobe conformation in the TbpA-hTf C-lobe structure.
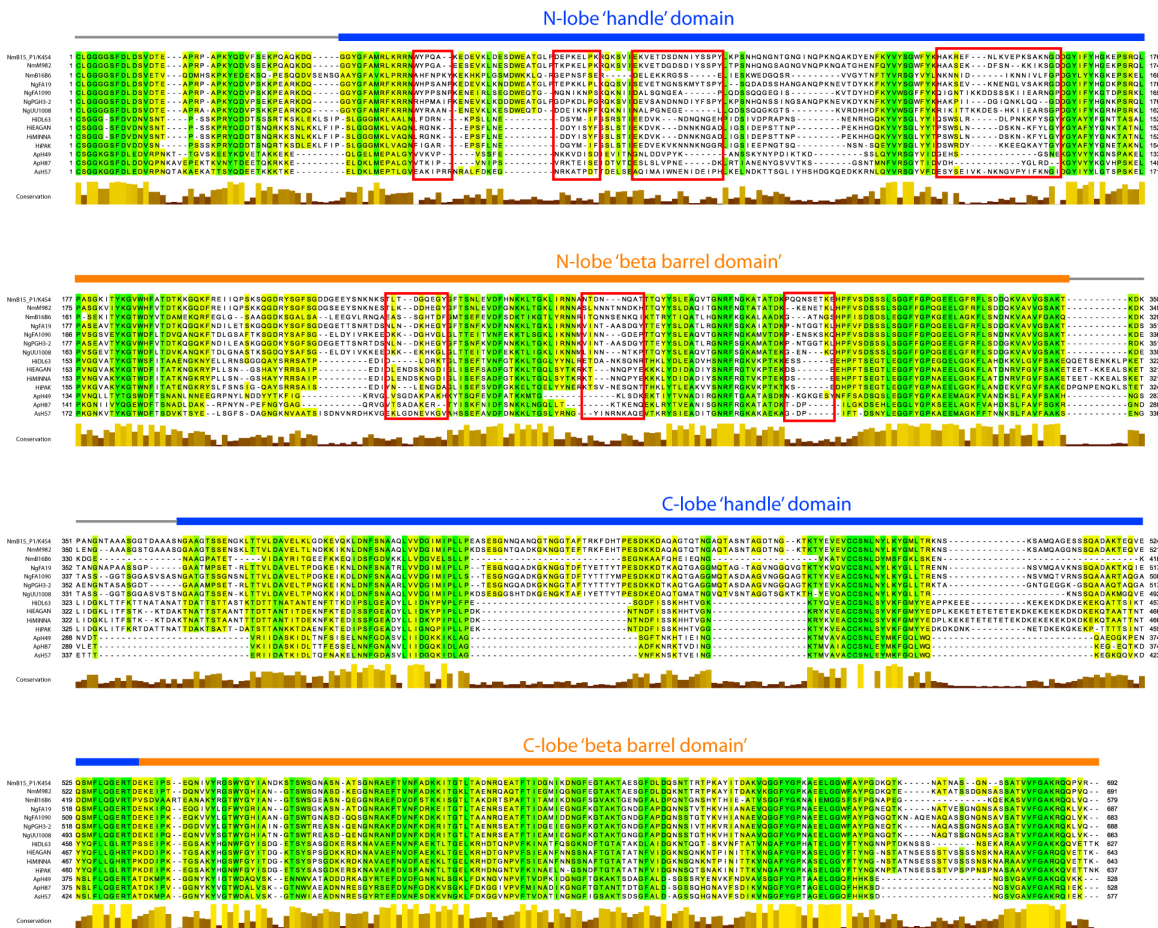
Figure S11: Sequence alignment of TbpB sequences from known pathogens. Residues are color coded according to conservation and conservation scores (Jalview) are indicated below the sequence. Domains are indicated above the sequence and sequences corresponding to the variable loop regions located along the binding interface with transferrin are outlined in red boxes. Abbreviations: *Neisseria meningitidis* (Nm); *Neisseria gonorrhoeae* (Ng); *Haemophilus influenzae* (Hi); *Actinobacillus pleuropneumoniae* (Ap); *Pasteurella haemolytica* (Ph); *Moraxella catarrhalis* (Mc).
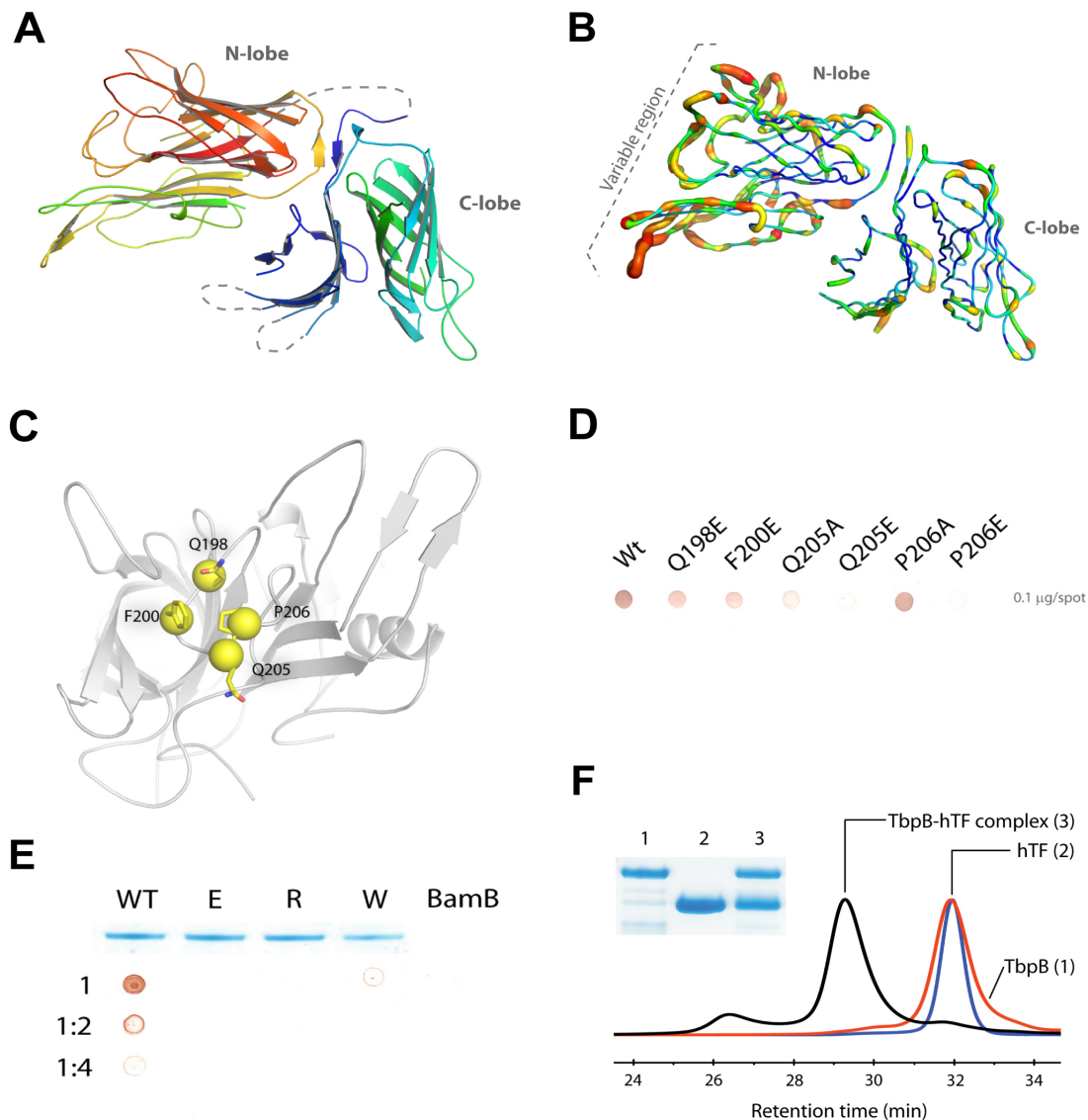
Figure S12. The crystal structure of Neisserial TbpB. A. The crystal structure of TbpB from *N. meningitidis* strain K454 (serogroup B) contains two lobes, each having an 8-strand beta barrel and additional strands that form a 'handle' domain. The N-lobe consists of residues 57-370, joined by a 32-residue linker to the C-lobe (residues 404-709). The unresolved density for the linker is consistent with considerable flexibility. Another 36-residue region connects the N-lobe barrel to the OM by a lipid anchor and may allow limited translational movement on the cell surface. TbpB is colored by rainbow with the N-terminus in red and the C-terminus in indigo. **B.** A putty conservation plot for TbpB illustrates the sequence variability found in human and porcine pathogens that express TbpB (refer to Fig. S9 showing sequence alignment for TbpBs). The most variable region, shown in red and orange, is primarily found in the N-lobe of TbpB, which is responsible for interacting with hTf. **C.** Mutations were made to disrupt hTf binding, targeting Q198, F200, Q205,

and P206, all structurally near porcine TbpB residue F171, where mutations abolished binding to pTf[4]. TbpB N-lobe is shown in gray cartoon and mutations are indicated by yellow spheres and sticks. **D.** We used dot blot assays to determine the levels of hTf-HRP binding in comparison to wild type TbpB. Here, we found that while each mutation affected binding to some degree, those mutations at positions 205 and 206 were the most effective in disrupting the interaction with hTf-HRP. Interestingly, mutating P206 to alanine had no effect, indicating that here, the conformational restraints characteristic of prolines were not significant to ordering the loop for interaction with hTf. **E.** A dot blot shows that mutating P206 to E, R, or W abolishes interaction with hTf. *E. coli* BamB was used as a control. **F.** Formation of the TbpB-hTf complex for SAXS analysis. The Coomassie stained SDS gel (inset) shows purified TbpB in lane 1 (orange elution profile), purified holo hTf in lane 2 (blue elution profile), and the complex isolated by size exclusion chromatography in lane 3 (black elution profile).
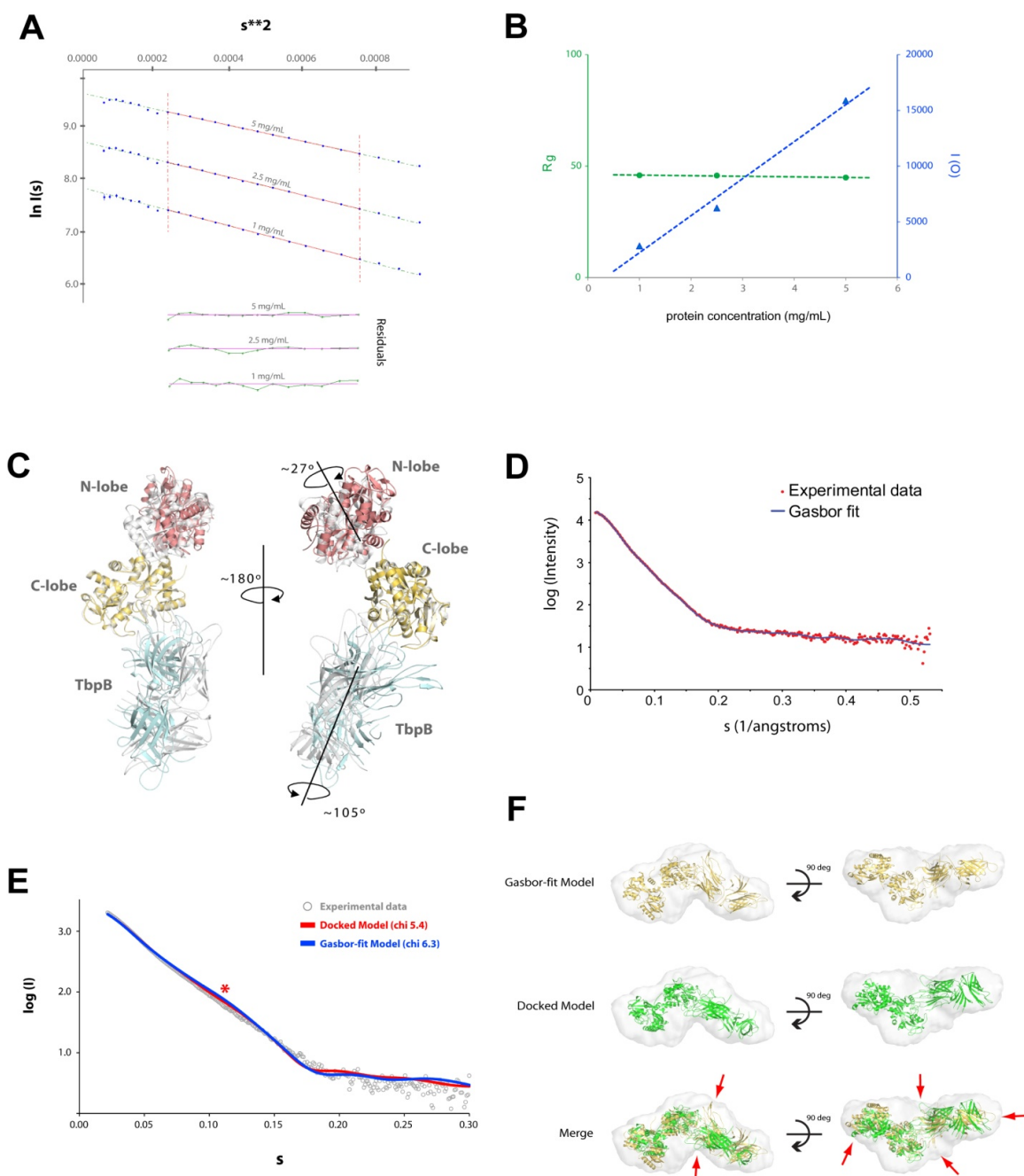
Figure S13. Fitting of the TbpB-(holo)hTf complex to the SAXS envelope. A. Guinier plot of the TbpB-hTf complex data at 1, 2.5, and 5 mg/mL. **B**. Plot of R_g and I(0) versus protein concentration. **C**. Superposition of the final TbpB-(holo)hTf complex (cyan, gold, and salmon) with our model obtained by docking the two known structures (gray), based on previous studies[4]. While the fit of the docked model was good, modifying the models produced a visually better fit to the envelope. Compared to the docked model, the N-lobe of hTf was rotated ~27°

relative to the C-lobe and TbpB was rotated ~105° to obtain the best fit to the SAXS envelope (optimized). Two views of the superposition, 180° apart, are shown. **D**. The SAXS molecular envelope was calculated using Gasbor. The experimental scattering is shown in red and *ab initio* Gasbor fit is shown in blue. **E**. Comparing the fit of the docked model and the optimized model to the experimental data using the program CRYSOL[5]. Here, the experimental data is show as gray circles, the fit for the back-calculation for the docked model is shown in red, and the optimized model is shown in blue. **F**. Comparison of the docked model and Gasbor-fit model docked into the *ab initio* calculated molecular envelope. The CRYSOL back calculated docked model shows a slightly better fit to the experimental data than does the Gasbor-fit model (see panel E asterisk and chi values), however, the Gasbor-fit model was optimized to fit the molecular envelope. The rationale for modifying the docked model as indicated is shown in the side-by-side comparison. Specific regions where the Gasbor-fit model showed improvement in overall fit are indicated by red arrows. It should be noted that special care was taken to preserve the interacting interface between the two molecules, which is based on mutagenesis studies of TbpBs from several different research groups (see Fig 3a). In addition, the calculated buried surface area of both models remains 1200-1300 $Å^2$ (PISA server) and conclusions for formation of the triple complex are unaffected by the choice of docked versus Gasbor-fit model.
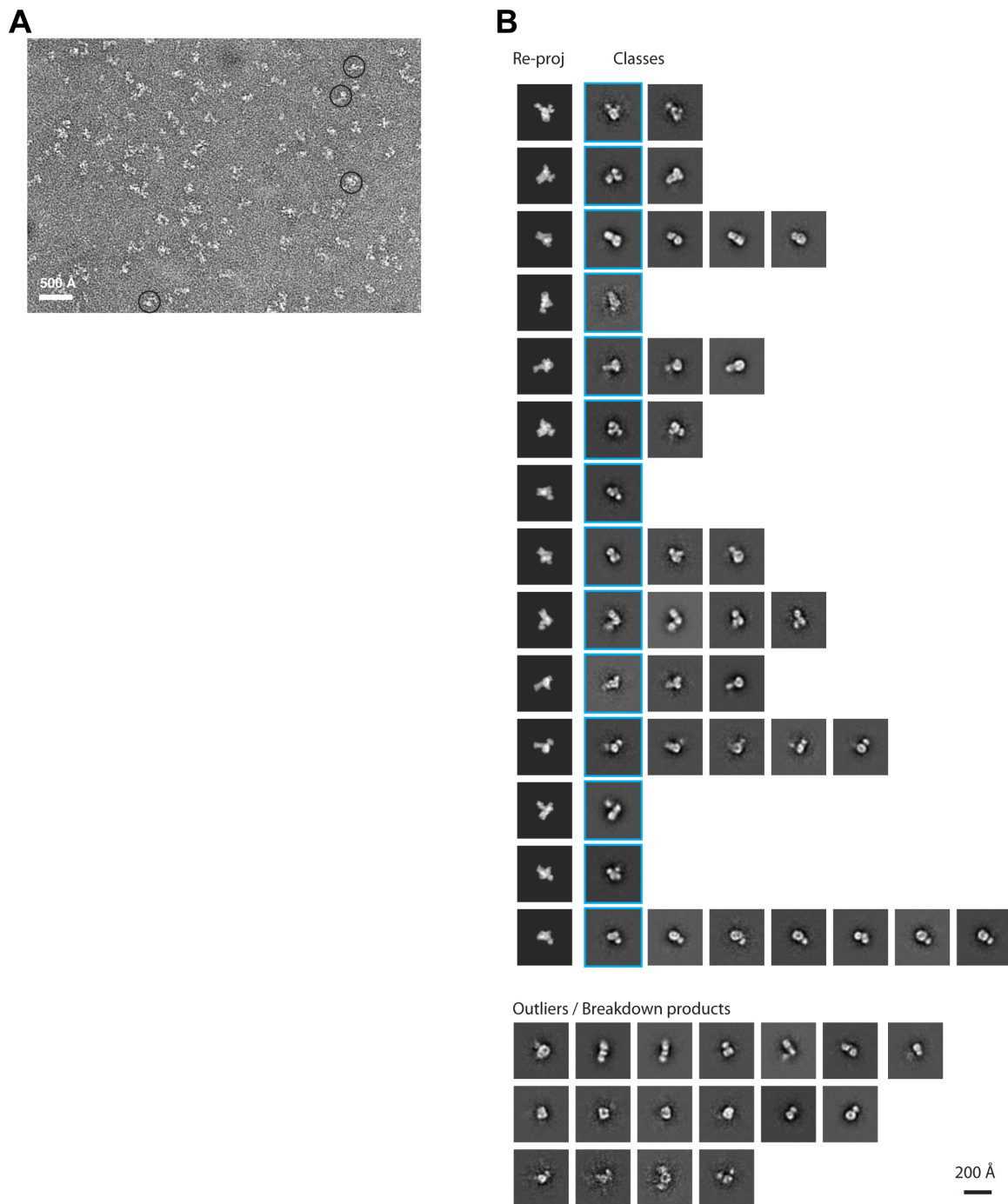
Figure S14: Electron microscopy analysis. A. Electron micrograph of a typical field of negatively stained TbpA-TbpB-(holo)hTf complexes. **B.** Class-average images obtained from a reference-free classification which yielded a total 56 of classes, with some redundancy. The class-averages were matched to a set of resolution-limited reprojections of the molecular model in equally spaced orientations (every 30˚) using SPIDER[6]. This produced a non-redundant set of 14

reprojections (first column) which are shown together with the corresponding class averages (second and subsequent images in each row. The observed redundancies probably reflect slight differences in viewing angle and/or staining. Some averages were excluded from this matching, according to the following criteria: [1] cross-correlation value to the best matched reprojection less than 0.7; [2] sizes too small for the best matched reprojection or otherwise not well compatible by visual criteria. These outliers, which account for < 25% of the picked particles, are in the two rows in the bottom panel. Four classes were too sparsely populated to merit further consideration.
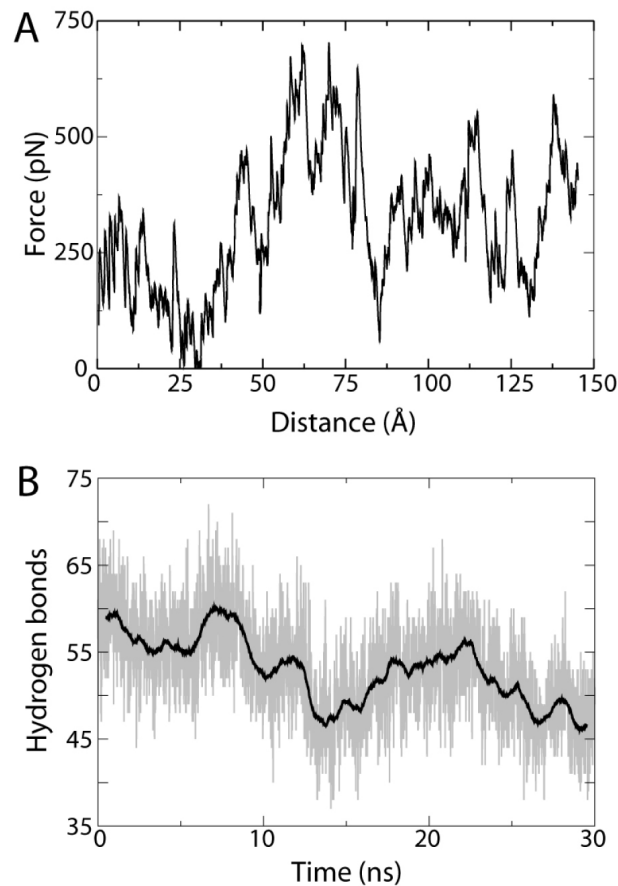
Figure S15. Simulated unfolding of the TbpA plug domain. This simulation characterized the formation of a regulated transmembrane pore formed in TbpA that could be exploited for iron transport. The design of the simulation was based on a proposed mechanism for active transport through force transduced by TonB to the transporter. The N-terminus of TbpA, located in the plug domain on the periplasmic side of the transporter, was pulled at a constant velocity of 5 Å/ns toward the cytoplasmic membrane using steered MD (see Methods). The force required to maintain a constant velocity was measured as a function of distance, plotted in (**A**). Force vs. distance. Plotted is the force required to pull the N-terminus of the plug domain at a constant velocity of 5 Å/ns away from the barrel. The curve represents a running average of window size 1000. Due to high pulling velocities, the forces are larger than those found in biological systems, although they correspond well with previous simulations[7]. Various peaks in the profile can be correlated with specific events in the unfolding process; for example, the initial broad set of peaks corresponds to "unzipping" of the first β-strand of the plug, the peak near 45 Å to the unfolding of the first helix, and that around 70 Å to the second helix. (**B**)

Hydrogen bonds vs. time. The black curve is a running average of the original data in light gray. Hydrogen bonds between the barrel and the plug decrease non-monotonically from 60 to 45 during plug extraction, nearly identical to observations made for a similar process in BtuB[7]. Unfolding was continued for a total of 30 ns, i.e., a distance of 150 Å. The result of force application *in vivo* is unlikely to be solely unfolding of the plug; at slower velocities a mix of unfolding and "unplugging", i.e., removal as a singular unit, is possible.
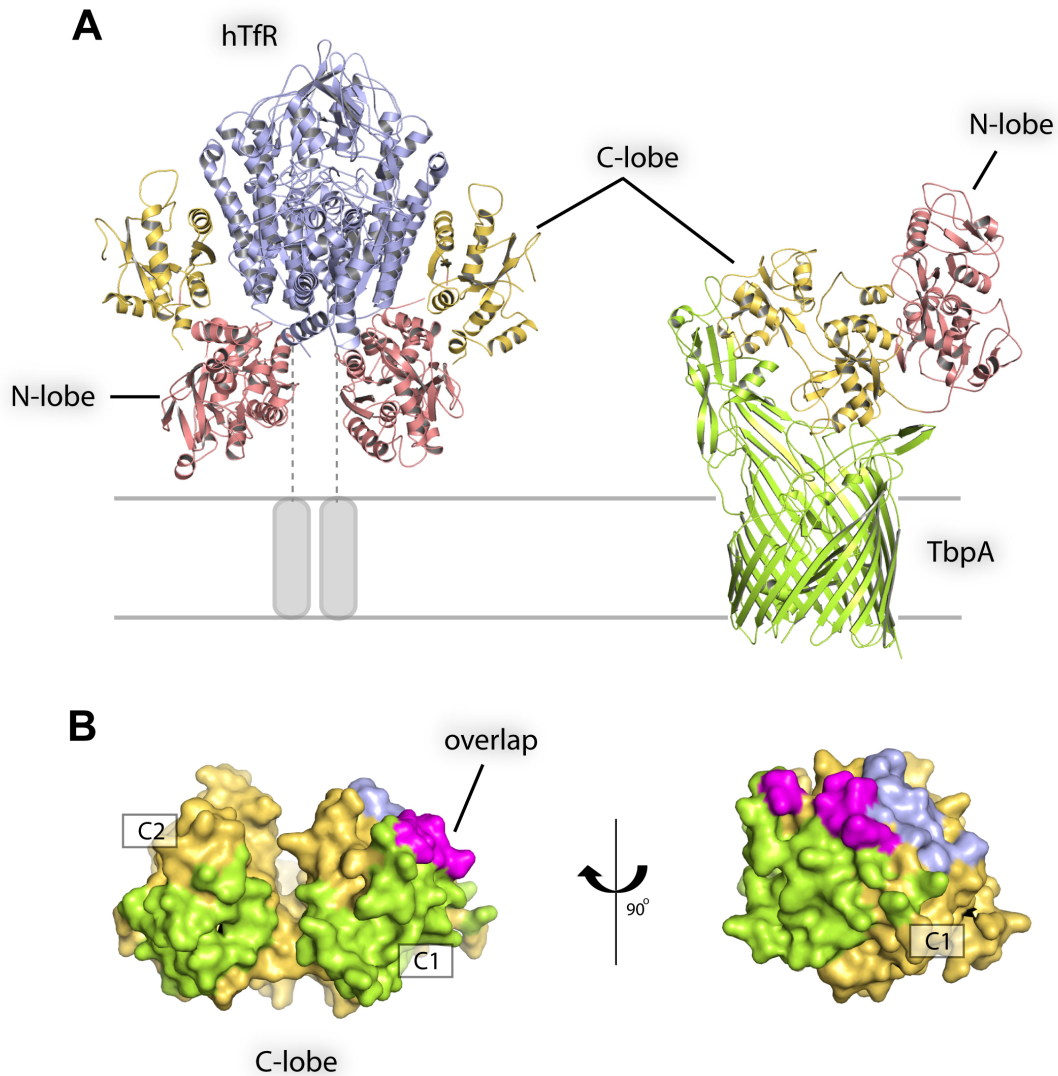
Figure S16: Comparison of hTf binding to the hTf-receptor from human and to TbpA from *Neisseria*. A. The structures of hTf in complex with the human transferrin receptor (hTfR) (PDB code 3S9L) and in complex with the *Neisserial* iron transporter TbpA. hTfR is shown in light blue ribbon, TbpA in green ribbon, and hTf shown in gold (C-lobe) and red (N-lobe). **B**. A surface representation of the hTf C-lobe with regions interacting with TbpA shown in green; regions interacting with hTfR shown in light blue; and regions that overlap the two binding sites shown in magenta. While hTfR interacts only with the C1-subdomain of hTf, TbpA interacts extensively with both C1- and C2-subdomains of hTf.

A.
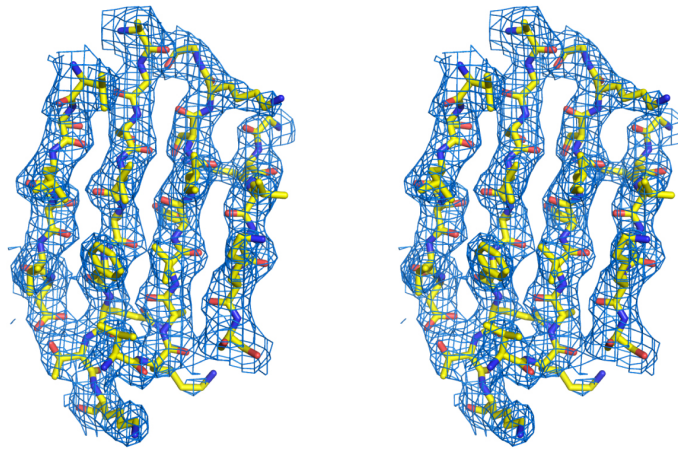
B.
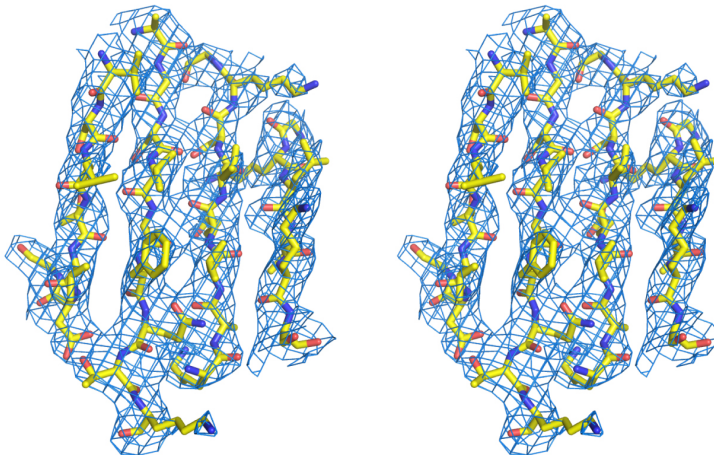
Figure S17: Electron density for the TbpA-(apo)hTf and TbpA-(apo)hTf C-lobe crystal structures. A. Stereo view of the electron density for the conserved four-strand beta sheet of the plug domain (residues 109-114, 168-176, 148-156, and 59-64) in the TbpA-(apo)hTf full-length structure (resolution 2.6 Å; PDB code 3V8X). **B.** Stereo view of the electron density for the same region of the plug domain in the TbpA-(apo)hTf C-lobe structure (resolution 3.1 Å; PDB code 3V89). Electron density maps are 2Fo-Fc maps contoured at 1σ.

A
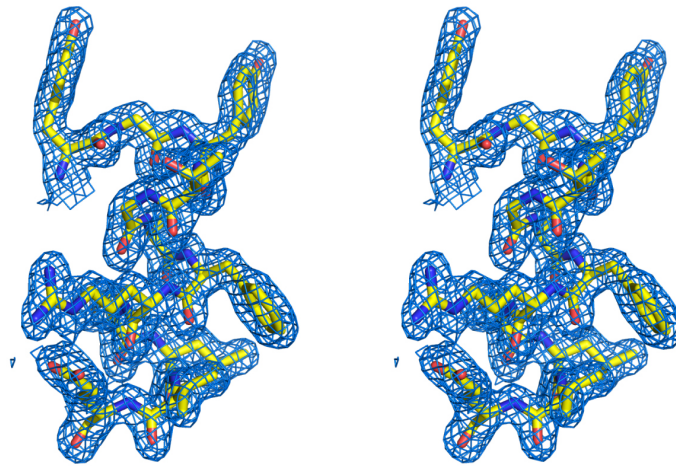
B
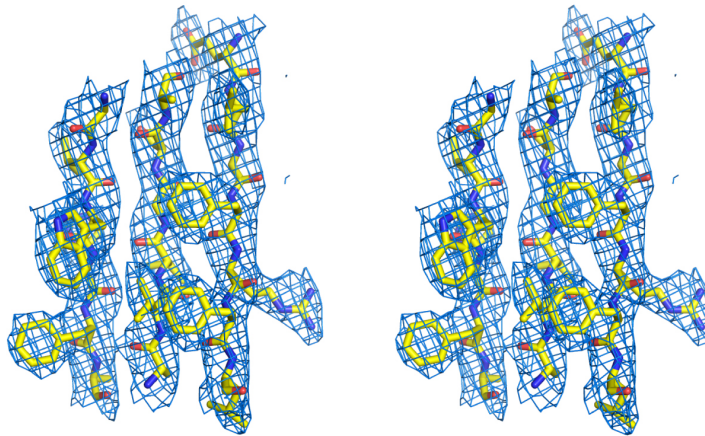
Figure S18: Electron density for the hTf C-lobe and TbpB crystal structures. A. Stereo view of the electron density for an alpha helix of the C2 domain (residues 515-526) of the (apo)hTf C-lobe structure (resolution 1.7 Å; PDB code 3SKP). **B.** Stereo view of the electron density for residues 61-67, 156-162, and 184-190 from the N-lobe of the TbpB structure (resolution 2.4 Å; PDB code 3V8U). Electron density maps are 2Fo-Fc maps contoured at 1σ.

Table S1: Data collection and refinement statistics

	TbpA-hTf	TbpA-hTf C-lobe	diferric hTf	apo hTf C-lobe	TbpB
Data Collection					
Space group	$P2_12_12_1$	$P2_1$	$C2$	$I422$	$P2_1$
a (Å)	91.01	58.06	254.53	95.85	75.29
b (Å)	129.36	107.59	173.00	95.85	82.76
c (Å)	198.59	130.72	150.15	204.14	111.88
α, (°)	90	90	90	90	90
β (°)	90	94.48	123.26	90	105.95
γ (°)	90	90	90	90	90
Resolution (Å)*	50-2.6 (2.69-2.6)	50-3.1 (3.21-3.1)	50-2.1 (2.18-2.1)	50-1.7 (1.76-1.7)	50-2.4 (2.49-2.4)
R_{sym}*	0.12 (0.84)	0.06 (0.24)	0.08 (0.46)	0.08 (0.83)	0.12 (0.54)
I/σI*	16.8 (1.5)	20.8 (3.9)	12.3 (1.7)	31.2 (2.2)	10.8 (1.7)
Completeness*	98.7 (97.4)	96.3 (76.9)	94.6 (91.5)	99.9 (99.9)	95.9 (92.4)
Redundancy*	4.5 (3.4)	3.7 (3.0)	2.5 (2.1)	7.0 (6.3)	4.4 (3.2)
Refinement					
Resolution (Å)	2.60	3.10	2.1	1.70	2.40
R_{work}/R_{free}	0.21/0.27	0.22/0.28	0.18/0.23	0.17/0.19	0.25/0.30†
Number of atoms					
Protein	11959	9168	31105	2608	8364
Ligand/ion	338	-	209	25	-
Water	190	-	2061	375	91
Average B-factors					
Protein	61.91	62.94	31.24	16.13	85.22
Ligand/ion	87.26	-	81.26	28.74	-
Water	52.47	-	32.3	30.56	60.72
R.m.s deviations					
Bond lengths(Å)	0.004	0.005	0.008	0.006	0.009
Bond angles(°)	1.101	1.125	1.147	1.015	1.429
PDB code	3V8X	3V89	3V83	3SKP	3V8U

* indicates statistics for highest shell shown in parenthesis

† R/R_{free} values are slightly higher than expected due to the detection of pseudotranslational symmetry (peak ~30% of the origin peak height in the Patterson map, PHENIX/Xtriage), which can lead to elevated R values.

Table S2: Summary of interactions between TbpA and hTf

TbpA	Group	Location	hTf	Group	Location	Distance*
Hydrogen bonds						
Gly 129	O	plug loop	Ser 415	N	C1	3.34
Asn 385	OD1	loop 3	Asp 416	N	C1	3.20
Ile 561	O	loop 5	Asn 417	ND2	C1	2.88
Tyr 255	O	loop 2	Lys 434	NZ	C2	3.36
Tyr 547	OH	loop 5	Lys 434	NZ	C2	2.99
Ala 361	O	loop 3	His 535	NE2	C2	3.20
Gln 360	O	loop 3	Gln 536	NE2	C2	3.26
Asp 251	OD1	loop 2	Asn 555	ND2	C2	2.77
Asn 367	O	loop 3	Lys 557	NZ	C2	3.39
Asn 367	OD1	loop 3	Lys 557	NZ	C2	3.35
Ser 538	OG	loop 5	Arg 568	N	C2	3.21
Ser 363	O	loop 3	Tyr 574	OH	C2	3.21
Ala 361	O	loop 3	Tyr 574	OH	C2	3.48
Gly 662	O	loop 7	Arg 602	NH2	C1	2.60
Asp 722	OD1	loop 9	Gln 603	NE2	C1	3.32
Arg 660	O	loop 7	His 606	ND1	C1	3.76
Arg 833	NH1	loop 11	Glu 357	OE1	C1	2.64
Asn 385	N	loop 3	Lys 414	O	C1	3.26
Lys 467	NZ	loop 4	Asp 416	OD1	C1	3.09
Thr 133	OG1	plug loop	Asp 416	OD1	C1	3.68
Tyr 515	OH	loop 5	Asp 416	OD1	C1	2.58
Asn 385	ND2	loop 3	Asp 416	OD2	C1	3.55
Thr 131	OG1	plug loop	Asp 416	OD2	C1	3.46
Thr 570	OG1	loop 5	Asn 417	OD1	C1	2.99
Asn 566	ND2	loop 5	Asp 420	OD1	C1	3.85
Lys 351	NZ	loop 3	Gly 543	O	C2	3.48
Ser 363	OG	loop 3	Glu 556	OE1	C2	2.56
Lys 358	NZ	loop 3	Glu 556	OE2	C2	3.46
Ser 253	OG	loop 2	Asp 558	OD1	C2	3.29
Gln 360	NE2	loop 3	Asp 634	OD2	C1	3.36
Salt Bridges						
Asp 355	OD1	loop 3	Lys 545	NZ	C2	3.37
Asp 279	OD1	loop 2	Lys 557	NZ	C2	3.11
Asp 722	OD1	loop 9	Lys 599	NZ	C1	3.41
Arg 833	NH1	loop 11	Glu 357	OE1	C1	2.64
Arg 833	NH1	loop 11	Glu 357	OE2	C1	2.74
Lys 467	NZ	loop 4	Asp 416	OD1	C1	3.09
Lys 467	NZ	loop 4	Asp 416	OD2	C1	3.10
Lys 358	NZ	loop 3	Glu 556	OE2	C2	3.46

Interactions were determined using the PISA server[8].

Other Interfacing Residues (TbpA)			
Gln 125	Ala 126	Ala 127	Leu 128
Ala 256	Val 280	Val 281	Asn 357
Pro 365	Gly 366	Gly 368	Lys 369
Ser 526	Thr 528	Ile 537	Pro 539
Tyr 569	Trp 659	Ala 661	Val 663
Gln 711	Lys 713	Ala 719	Lys 720
Asp 777	Arg 825	Leu 827	Leu 828
Lys 836	Ala 884	Gln 890	Lys 892
Gly 130	Ser 252	Asn 254	Asn 893
Lys 359	Gly 362	Leu 364	Asn 831
Gly 383	Glu 384	Tyr 524	Asn 834
Asn 540	Arg 563	Thr 568	Thr 835
Gln 664	Arg 706	Tyr 708	Thr 776
Gly 721	Pro 723		

Other Interfacing Residues (hTf)			
Ala 334	Thr 336	Glu 338	Lys 340
Val 363	Gly 364	Gly 365	Tyr 412
Thr 421	Ser 435	Lys 534	Pro 539
Lys 569	Pro 570	Val 571	Glu 572
Gln 604	Gln 605	Leu 607	Phe 608
Val 612	Thr 613	Asp 614	Ser 616
Val 360	Asn 361	Ser 362	Lys 640
Asn 413	Cys 418	Glu 419	Cys 637
Gln 540	Glu 560	Thr 567	Val 636
Glu 573	Ala 575	His 598	Asn 618
Gly 609	Ser 610	Asn 611	Gly 617

* in angstroms (Å)

Table S3: Sequences for the plug loop and extracellular loops in TbpA

Loop	Length	Loop sequence
1	4	GKNR
2	76	EIRAHEDAGRGVQSFNRLVPVEDSSNYAYFIVKEE**C**KNGSYET**C**KANPKKDVVGKDERQ TVSTRDYTGPNRF LADP
3*	54	DMTVPAFLTKAVFDANKK<u>QAGSLPGNGKYAGNHK</u>YGGLFTNGENGALVGAEYGT
4	17	**C**SADGSDKY**C**RPSADKP
5	54	NRAYSSNTPPQNNGKKISPNGSETSPYWVTIGRGNVVTGQI**C**RLGNNTYTD**C**TP
6	12	SDDGSVSTGTHR
7*	23	LPSFA<u>EMYGWRAGVQSKAVKIDP</u>
8	18	GYEAQIKDGKEEAKGDPA
9	18	RADRTDIQSHLFDAIQPS
10	31	KAKEITELLGSRALLNGNSRNTKATARRTRP
11*	38	NLLNYRYVTWENVRQT<u>AGGAVNQHKNVGVYNRY</u>AAPGR
Plug Loop*	14	<u>TAQAALGGTRTAGS</u>

* These loops were used for polyclonal antibody development with underlined
sequences as the representative antigens.

Table S4: Sequence analysis of the plug loop and extracellular loops in TbpA from known pathogens

Loop	strain	L1	L2	L3	L4	L5	L6	L7	L8	L9	L10	L11	PL
1	Nm-B15-P1 (K454)	Reference (% sequence identity)											
2	Nm-B16B6	50	67	48	70	58	83	65	44	72	67	100	100
3	Nm-M982	100	88	98	100	76	100	95	94	100	100	100	100
4	Ng-UU1008	100	85	79	100	74	100	82	77	100	100	94	100
5	Ng-FA1090	100	86	79	100	83	100	82	88	100	96	94	100
6	Ng-4102	100	85	79	100	72	100	82	83	100	100	94	100
7	Ng-FA19	100	85	90	100	75	100	82	83	100	100	94	100
8	Ng-PGH3-2	100	80	92	100	89	100	82	77	100	100	94	100
	Average (1-8)	93.8	84.5	83.1	96.3	78.4	97.9	83.8	80.8	96.5	95.4	96.3	100
9	Hi-EAGAN	50	36	20	52	18	16	52	20	55	60	81	14
10	Hi-DL63	50	39	25	52	26	16	56	18	55	63	84	14
11	Hi-MINNA	50	36	20	52	18	16	52	20	55	60	81	14
12	Hi-PAK	50	39	25	52	16	16	56	20	55	60	81	14
13	Ap-H49	50	25	14	47	13	25	39	8	41	30	65	12
14	Ap-H171	50	30	9	47	13	25	39	8	41	30	65	12
15	Ph-H196	50	19	22	52	20	41	30	7	27	21	51	25
16	Mc-4223	50	43	20	47	25	25	52	27	47	38	63	21
17	Mc-Q8	50	43	22	47	25	25	52	27	47	38	63	21
	Average (1-17)	72.2	60.3	52.3	73.2	50.0	60.4	66.5	50.0	71.9	70.1	83.5	58.1

Abbreviations: *Neisseria gonorrhoeae* (Ng); *Neisseria meningitidis* (Nm); *Haemophilus influenzae* (Hi); *Actinobacillus pleuropneumoniae* (Ap); *Pasteurella haemolytica* (Ph); *Moraxella catarrhalis* (Mc); Plug loop (PL).
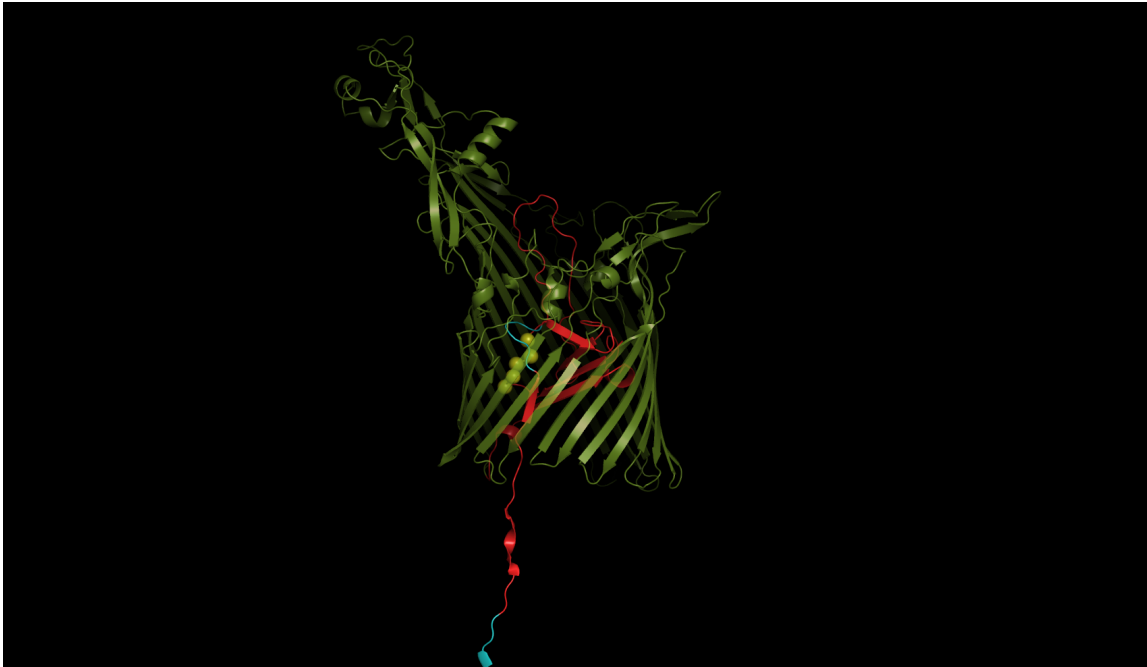
Movie S1: Molecular dynamics simulation of the TbpA-TonB interaction. This movie shows the results of the molecular dynamics simulations that were designed to mimic interactions with the TonB system. The conformational changes within the plug domain were monitored and analyzed for the formation of a pore that potentially represents a pathway for iron transport. Electrostatics of the cavities are visualized and found to be very dynamic during the simulations. The electrostatics of the proposed iron import pathway change significantly during the simulation, beginning highly electronegative (promoting iron import), becoming more neutral, and finally becoming electropositive, which may assist in ejecting iron from the barrel domain into the periplasm.
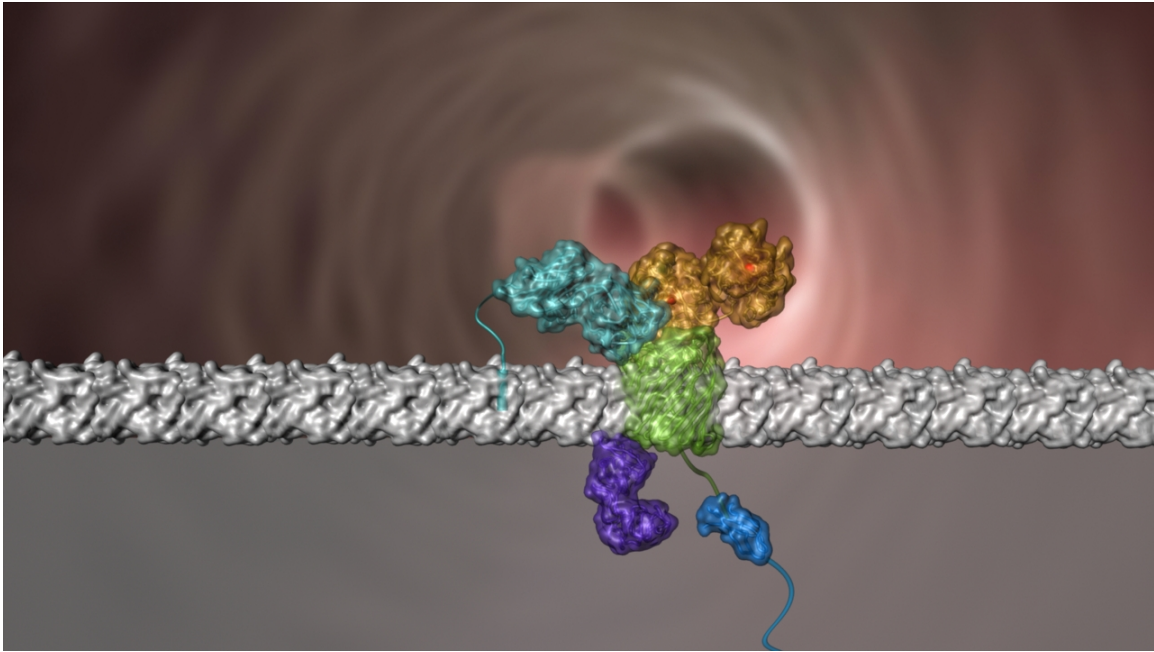
Movie S2: The iron import machinery from pathogenic *Neisseria*. This movie shows how *Neisseria* are able to extract iron from transferrin for transport across the outer membrane. While TbpB presumably dissociates from hTf once iron is released, the mechanism for dissociation of apo-hTf from TbpA is not known. Two plausible mechanisms are as follows: [1] a second TbpB-(holo)hTf complex may compete off apo-hTf from TbpA, or [2] a signal from the plug domain may initiate ejection of apo-hTf (depicted in the movie).

References

1. Ashkenazy, H., Erez, E., Martz, E., Pupko, T. & Ben-Tal, N. ConSurf 2010: calculating evolutionary conservation in sequence and structure of proteins and nucleic acids. *Nucl Acids Res* **38**, W529-33 (2010).
2. Waterhouse, A. M., Procter, J. B., Martin, D. M., Clamp, M. & Barton, G. J. Jalview Version 2--a multiple sequence alignment editor and analysis workbench. *Bioinformatics* **25**, 1189-91 (2009).
3. Cornelissen, C. N., Anderson, J. E., Boulton, I. C. & Sparling, P. F. Antigenic and sequence diversity in gonococcal transferrin-binding protein A. *Infect Immun* **68**, 4725-35 (2000).
4. Moraes, T. F., Yu, R. H., Strynadka, N. C. & Schryvers, A. B. Insights into the bacterial transferrin receptor: the structure of transferrin-binding protein B from Actinobacillus pleuropneumoniae. *Mol Cell* **35**, 523-33 (2009).
5. Svergun, D. I., Barberato, C. & Koch, M. H. J. CRYSOL - a Program to Evaluate X-ray Solution Scattering of Biological Macromolecules from Atomic Coordinates. *J Appl Crystallogr* **28**, 768-773 (1995).
6. Shaikh, T. R. et al. SPIDER image processing for single-particle reconstruction of biological macromolecules from electron micrographs. *Nat Protocols* **3**, 1941-74 (2008).
7. Gumbart, J., Wiener, M. C. & Tajkhorshid, E. Mechanics of force propagation in TonB-dependent outer membrane transport. *Biophys J* **93**, 496-504 (2007).
8. Krissinel, E. & Henrick, K. Inference of macromolecular assemblies from crystalline state. *J Mol Biol* **372**, 774-97 (2007).